Atomic scale DFT simulations of point defects in uranium nitride

2007 J. Phys.: Condens. Matter 19 106208

(http://iopscience.iop.org/0953-8984/19/10/106208)

IOP PUBLISHING JOURNAL OF PHYSICS: CONDENSED MATTER

J. Phys.: Condens. Matter **19** (2007) 106208 (9pp) doi:10.1088/0953-8984/19/10/106208

Atomic scale DFT simulations of point defects in uranium nitride

E A Kotomin[1], R W Grimes[2], Y Mastrikov[3] and N J Ashley[2]

[1] European Commission, Joint Research Centre, Institute for Transuranium Elements, PO Box 2340, D-76125, Karlsruhe, Germany
[2] Department of Materials, Imperial College London, SW7 2BP, UK
[3] Institute of Solid State Physics, University of Latvia, Kengaraga 8, Riga, LV-1063, Latvia

Received 5 December 2006, in final form 5 January 2007
Published 16 February 2007
Online at stacks.iop.org/JPhysCM/19/106208

Abstract

Atomic scale density functional calculations are used to predict the behaviour of defects in uranium mononitride (UN). Two different density functional codes (VASP and CASTEP) were employed with supercells containing from 8 to 250 atoms (providing a significant range of defect concentrations). Schottky and nitrogen Frenkel point defect formation energies, local lattice relaxations and overall lattice parameter change, as well as the defect induced electronic density redistribution, are discussed.

(Some figures in this article are in colour only in the electronic version)

1. Introduction

Actinide nitrides have been studied experimentally because they have some advantages over oxides as fuel materials for fast reactors. In particular, they exhibit higher thermal conductivity and higher metal density [1–3]. Recently there has been renewed interest in these materials because of the Generation-IV reactor initiative [4]. In order to predict fuel performance under different operating conditions and to understand the evolution of a spent fuel over long times in a repository, it is necessary to develop a better knowledge of the defect induced processes caused by material self-irradiation and the accumulation of fission products. Defect modelling studies have been performed for oxide fuels over several decades, first using classical [5–7] and recently first principles quantum mechanical methods [8, 9]. Conversely, for nitrides, to date only a preliminary first principles LMTO simulation of pure UN has been reported [10], and a single molecular dynamics study [11]. The purpose of this paper is to report first principles calculations of point defects in UN and analyse their properties.

2. Methodology

In our simulations of perfect and defective uranium nitride, two different plane wave basis set density functional theory (DFT) computer codes were employed, VASP 4.6 [12] and

Table 1. A comparison of calculated (PW91(PAW) and PW91(US)) and experimental perfect lattice properties [1, 2, 16, 21, 22] of UN, U_2N_3 and UN_2.

	PW91(PAW)			PW91(US)		
Lattice properties	UN	U_2N_3	UN_2	UN	U_2N_3	UN_2
Lattice constant, a_0 (Å)	4.864	3.647	5.259	4.954	3.741	5.256
(0 K)		5.802			5.722	
Experimental a_0 (Å)	4.886	3.700	5.299	4.886	3.700	5.299
		5.825			5.825	
Bulk modulus, B (GPa)	203	208.9	264.6	182	153.6	235.8
Experimental B (GPa)	194	—	—	194	—	—
Cohesive energy, E_0 (eV)	14.7	36.27	21.50	12.3	30.1	17.9
Experimental E_0 (eV)	13.6	—	—	13.6	—	—
Q (U) (e)	1.66	2.08	2.48	—	—	—
Q (N) (e)	−1.66	−1.50,	−1.24	—	—	—
		−1.34				

CASTEP [13]. In both cases exchange–correlation was described using the Perdew–Wang-91 GGA functional [14]. For the VASP calculations the scalar relativistic PAW pseudopotentials were used to represent the core electrons of U ($6s^2 6p^6 6d^2 5f^2 7s^2$) and N ($2s^2 2p^3$) atoms, which therefore have 14 and 5 valence electrons respectively. The CASTEP calculations used the same valence electron sets as the VASP calculations but employed an ultrasoft pseudopotential (US) representation to describe the core electrons. Both codes used a plane wave cut-off energy of 400 eV, with a 3 × 3 × 3 Monkhorst–Pack [15] k-point mesh in the Brillouin zone for supercells containing 16 atoms and more, and 8 × 8 × 8 k-sets for primitive unit cells and eight atom supercells. Hereafter, we refer to these two types of calculation as PW91(PAW) and PW91(US), respectively. Further increase of the number of the k-points does not change the results.

Stoichiometric UN exhibits the rock-salt structure with two atoms per primitive unit cell. In the PW91(PAW) calculations, point defects were simulated using supercells with 2 × 2 × 2, 3 × 3 × 3, 4 × 4 × 4 and 5 × 5 × 5 extended translation vectors of the primitive unit cell with complete structure optimization (16, 54, 128 and 250 atoms per supercell, respectively). In addition we used an eight atom single cubic unit cell. Neutral vacancies were modelled by removing a U or N *atom* from the supercell to infinity (the reference state) to form V_N or V_U. Nitrogen Frenkel defects were described by moving a N atom from a regular site into the interstitial position in the cube centre, at the distance of 8.6 Å from the vacancy in the 128 atom supercell. Lastly, the very large 5 × 5 × 5 supercell was used to model a pair of well separated N and U vacancies. As with all the defect simulations, this was accompanied by a complete atomic and electronic structural optimization. The PW91(US) point defect calculations were performed, for comparison, using an eight atom cubic unit cell (with complete atomic and electronic structural optimization).

3. Results of calculations

3.1. Perfect UN crystal

Perfect stoichiometric UN was modelled using both PW91(PAW) and PW(US) approaches, and in table 1 results are compared to experimental data [1, 16]. This shows that both methods were able to successfully reproduce the basic properties of the material (lattice constant, bulk modulus and cohesive energy). The effective (Bader) charges Q calculated using VASP [17]

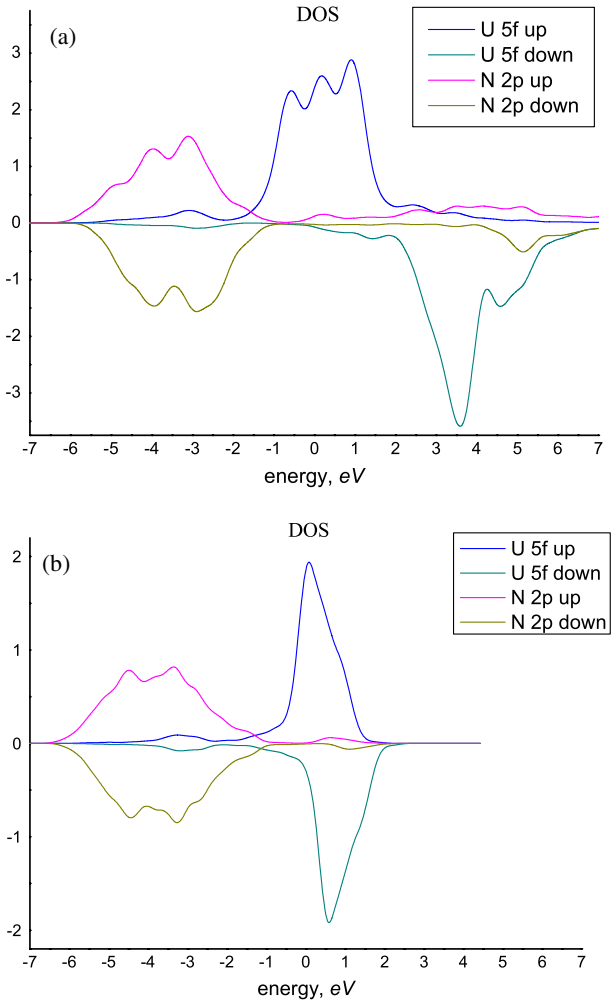

Figure 1. Calculated density of states (in arbitrary units) for primitive unit cells of UN projected onto U 5f and N 2p orbitals for the spin up (above) and spin down (below); the zero of energy is the Fermi energy; (a) CASTEP, (b) VASP.

are $\pm 1.6e$ which is indicative of the complex chemical bonding, with covalency contributions due to U 5f and N 2p orbital hybridization, observed in the projected density of states (DOS; see figure 1). Charge transfer from U atoms towards nearest N atoms, which retain their spherical shape, is clearly seen in figure 2, the difference electron density map. This is consistent with discussions in previous theoretical [10] and experimental [18, 19] studies that described the mixed metallic–covalent chemical bonding in UN; this is quite different to the semiconducting nature of UO_2 [20]. The observed difference in results (e.g. unoccupied DOS for U 5f states and lattice constants) could be caused by difference in pseudopotentials used in CASTEP and VASP calculations.

3.2. Stoichiometric compounds of uranium and nitrogen

Further calculations on experimentally known relevant stoichiometric compounds (U_2N_3 [21] and UN_2 [22]) were also carried out. Again both codes were able to successfully reproduce

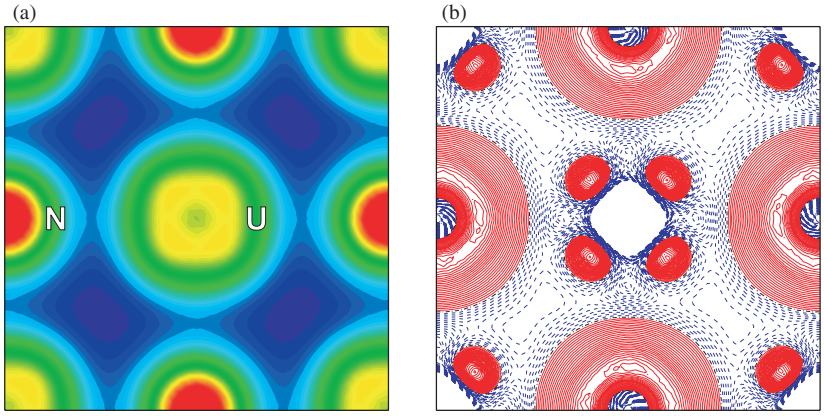

Figure 2. (a) The total electron density of defect free UN calculated using VASP; (b) the difference between the self-consistent perfect crystal density and that of a superposition of the U and N atomic densities. Red (full lines) indicate electron density excess, blue (dashed) its deficiency. The electronic density increment is $0.005e$ Å^{-3}.

the lattice parameters of these materials (as shown in table 1). Of particular interest are the predicted changes in effective charges as a function of decreasing U:N ratio (from UN to UN_2). It appears that the uranium charge increases while the nitrogen charge decreases, which indicates a significant propensity for charge transfer dependent on the local atomic arrangement[4].

3.3. Single defect calculations

The first two columns in table 2 report the internal energies of formation, E^{form}, for V_{U} and V_{N} calculated using three different cells containing 8, 16 and 54 atoms respectively. For V_{N} the energy is calculated via

$$E^{\text{form}}(V_{\text{N}}) = E^{\text{def}} + E(N) - E^{\text{perf}}$$

where $E(N)$ is the energy for a spin-polarized isolated nitrogen atom. In each case, a single atom has been removed.

The first column presents energies from calculations in which the cell parameters and atom positions remain fixed in their perfect lattice positions, that is, atoms are not allowed to relax in response to defect formation (unrelaxed). Energies in the second column are derived from calculations that allowed full lattice relaxation. The top two rows of numbers, calculated using the largest cell, correspond to a 3.7% V_{N} or V_{U} concentration and include the smallest defect–defect interaction (via the periodic conditions). The differences between the unrelaxed and relaxed lattice formation energies are the relaxation (or response) energies. For the largest cell these are similar: 1 eV for V_{U} and 0.7 eV for a V_{N}. The response of the lattice to defect inclusion can also be assessed by considering the difference in macroscopic unit cell dimension between perfect (a_0) and defective materials (see table 2). Interestingly, at this low concentration the V_{N} has little effect on the lattice constant, a 0.17% a_0 compression, while the V_{U} causes a slightly larger compression of 0.21% a_0.

[4] Note: CASTEP at present does not predict topological (Bader) charges, only Mulliken ones. Although Mulliken populations calculated for UN, U_2N_3 and UN_2 using CASTEP showed very similar changes as a function of U:N ratio, because of the inherent uncertainties of Mulliken populations derived from plane wave calculations we chose not to report charges here.

Table 2. Calculated defect properties: formation energies, E^{form} for V_{U} and V_{N} defects before and after relaxation of the lattice; changes to the lattice constant, a_0, upon relaxation as a % of a_0 (negative values imply that the lattice has compressed); total change in supercell volume due to defect formation; local displacements of nearest neighbour atoms around vacancies (negative values imply inward movement).

Defect/supercell	E^{form} (eV) (unrelaxed)	E^{form} (eV) (relaxed)	Cell dimension change % of a_0	Defect volume (Å^3)	Nearest neighbour displacement (Å)
PW91(PAW) 54 atom cell (3.7%)					
N vacancy	9.8	9.1	−0.17	3.94	−0.03 (−0.05)[a]
U vacancy	10.4	9.4	−0.21	4.75	0.13 (0.14)[a]
PW91(PAW) 16 atom cell (12.5%)					
N vacancy	10.7	9.7	−0.60	3.38	−0.01
U vacancy	11.2	10.3	−1.02	6.88	0.10
PW91(PAW) 8 atom cell (25%)					
N vacancy	9.3	9.1	−1.00	3.37	None[b]
U vacancy	10.7	10.1	−3.39	10.58	None[b]
PW91(US) 8 atom cell (25%)					
N vacancy	8.8	8.8	−0.58	2.11	None[b]
U vacancy	11.7	9.3	−2.61	9.27	None[b]

[a] 250 atom supercell containing both vacancies.
[b] By symmetry.

Given the small global effect at the low defect concentration (i.e. on relaxation energy and cell dimension), defect calculations were also performed at the much higher concentrations of 12.5% and even 25% (see table 2). Interestingly the defect formation energies do not reveal any considerable dependence on the concentration. (The energies calculated using the PW91(US) are slightly smaller but reveal the same trend.) Despite the very large defect concentrations, the cell dimension decreased by only 0.6% (at 12.5%) and 1.0% (at 25%) for V_{N} and by 1.0% (at 12.5%) and 3.4% (at 25%) for V_{U}. Thus, for the V_{N} defect, the increase in lattice parameter is almost a linear function of the defect concentration. For the V_{U} the situation is slightly different. First, at larger concentrations it affects the lattice constant more than does V_{N}. Furthermore, the increase in lattice parameter with defect concentration deviates from a linear response. The PW91(US) calculations give similar but smaller lattice constant changes to PW91(PAW) at 25% defect concentrations (see table 2).

In order to better compare the effects of different concentrations, the change in cell dimension is translated into a *defect volume*. These are the total changes in volume (Å^3) imparted by the defect and are reported in table 2. The linear increase in lattice parameter with defect concentration is evident in that the three different simulation sizes give rise to similar V_{N} volumes of around 3.5 Å^3. Of course, the constancy of this value would only arise if the nitrogen defect had a very local influence on the lattice. Similar effects have been predicted in ZrN and TiN [23] and lead to the experimentally observed stability of these nitrides over extensive ranges in nitrogen nonstoichiometry.

The V_U defects induce larger defect volumes, which also increase markedly with defect concentration: from 4.75 to 10.58 Å^3. The PW91(US) calculations also predict defect volumes that are much larger for V_U than V_N.

In order to investigate the *local* effects of defect inclusion, the atomic displacements around defects were also investigated (last column in table 2). For V_N this corresponded to a 0.67% *inward* displacement of the six nearest U atoms at a 3.7% vacancy concentration, with smaller 0.49% inward displacements at the 12.5% vacancy concentration. At both defect concentrations the second neighbour N atoms remain practically at their perfect lattice sites.

In contrast, the six nearest N atoms around the V_U are displaced *outwards* by 2.69% at a 3.7% vacancy concentration, and at 12.5% they are moved by 2.04%. Furthermore, twelve second neighbour U atoms are displaced inwards by 0.75% and 0.57% respectively. Nevertheless, as for the V_N the trend is for a decrease in relaxation of defect nearest neighbour atoms with increasing defect concentration, due to defect–defect interactions. It is interesting to contrast the change in significant local atom relaxation direction between V_N and V_U with the observation of overall lattice contraction for both defects.

The second way in which local effects have been investigated is by generating electron density difference maps (see figure 3). For the V_N, figure 3(a) shows that the electron density from the missing N atom is almost entirely localized on the six nearest neighbour U atoms. In the case of the V_U (figure 3(b)), the electronic density redistribution is more spread out over the immediate vicinity. This is confirmed by the Bader effective charges: in the 54 atom cell an additional charge of $0.22e$ is transferred from the missing N atom onto each of six U ions. In comparison a hole density of $0.16e$ is transferred from the missing U atom onto each of the nearest N ions; the remaining positive density is transferred to more remote ions.

We also made calculations for *a pair* of well separated U and N vacancies in a 250 atom supercell. Atomic displacements around each vacancy are similar to those obtained in separate defect calculations at a 3.7% defect concentration (see table 2).

3.4. Frenkel and Schottky pairs

The PW91(PAW) calculations of the internal energies for forming intrinsic Frenkel and Schottky defect pairs using an unrelaxed 128 atom supercell yield values of 6.9 and 5.5 eV respectively. That is, the Frenkel energy is somewhat higher than the Schottky energy, reflecting the compact nature of the rock-salt lattice that provides little space for an interstitial defect. Subsequently when lattice ions are allowed to relax in response to defect inclusion, these energies are reduced to 4.6 and 3.8 eV so that, while the Schottky energy is still lower, the difference is rather less. Furthermore, the Schottky energy obtained using the 250 atom supercell, 4.4 eV, is slightly higher and even closer to the Frenkel energy. Although for this largest simulation the two vacancies are included in the same 250 atom supercell, the observed displacements of atoms around the individual defects are very similar to those observed in the separate 54 atom supercell calculations (see table 2).

In oxides and halides with the rock-salt structure, the Frenkel energy is larger than the Schottky energy even with full lattice relaxation [24]. To investigate why this is not the case here, the charge distribution of the Frenkel pair was analysed. Interestingly it showed quite complex electron density redistribution (see figure 4). In particular, the electron density that the interstitial N atom gains from its nearest neighbours, which results in an effective charge of $-1.07e$, is considerably less than that in a host crystalline site ($-1.6e$). To demonstrate this result, we plotted in figures 4(b) and (c) the difference maps with respect to the isolated N atom and ion, respectively. The effective charge of $-1e$ for the interstitial nitrogen ion is in good agreement with an indirect conclusion based on experimental observations [19].

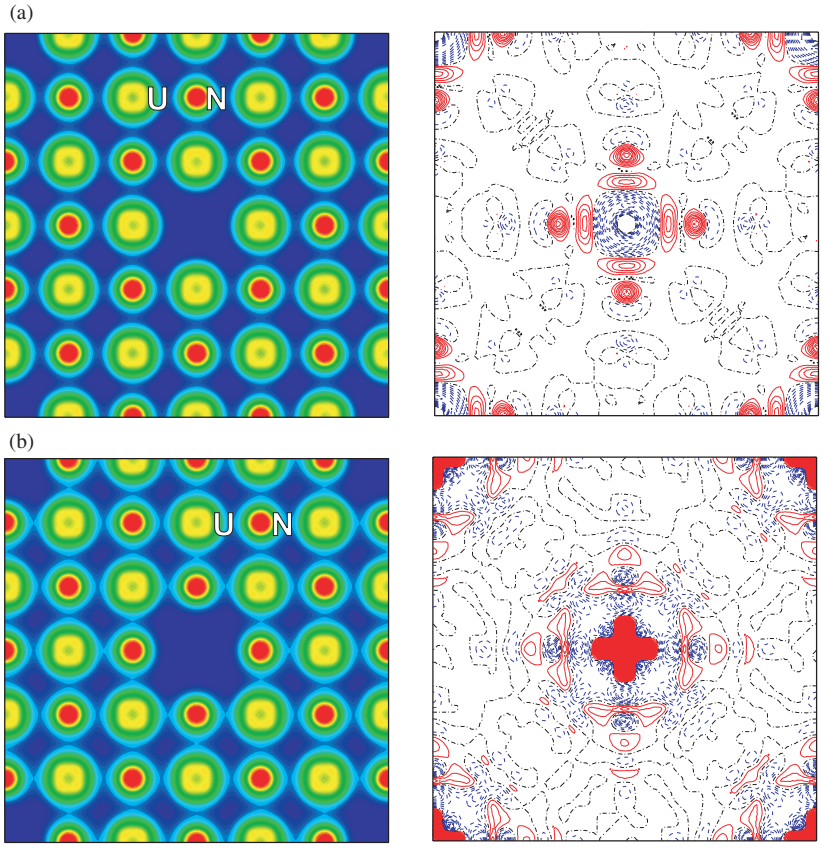

Figure 3. (a) The total (left) and difference (right) electron densities around the V_N. The latter is the difference of the self-consistent total density for a defective crystal minus a sum of the density of a single N atom centred on the vacancy and the density of the defective crystal. The electron density of a missing N atom (blue, dashed lines) is transferred to the six nearest U atoms (red, full lines). (b) is the equivalent for a V_U defect. The density increment is $0.01e$ Å^{-3}.

4. Conclusions

This study has demonstrated that atomic scale DFT-GGA-PW91 plane wave calculations with scalar relativistic pseudopotentials as implemented in the VASP and CASTEP codes (combined with a supercell approach) can be used successfully to model a series of uranium nitride perfect lattice structures and also point defects in uranium mononitride. The only difference between the two sets of calculations was in the pseudopotentials employed: PAW (VASP) versus ultrasoft pseudopotentials (CASTEP). Certain differences that arose in the results are attributed to this.

We have shown that V_N defects have hardly any effect on the UN lattice constant, even for concentrations as high as 25%. For this defect the lattice response is confined to small inward displacements of the nearest neighbour uranium ions and a very local defect induced electronic density redistribution. This response to the formation of a vacancy is more reminiscent of a metal than an ionic or semiconducting material (e.g. UO_2). Conversely, V_U defects induce somewhat larger (but still small) defect volumes, which increase in magnitude as a function of defect concentration. In this case the nearest neighbour nitrogen atoms are displaced outwards

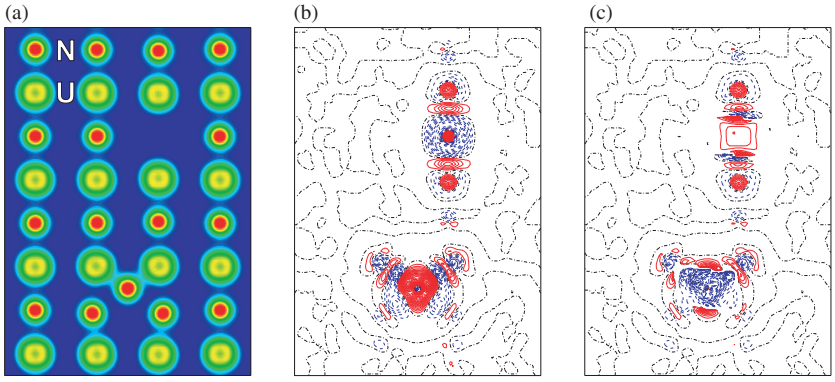

Figure 4. A (110) cross-section of (a) the total and ((b), (c)) the difference electron density of the Frenkel pair. The interstitial atom (in the lower part) is strongly polarized, along with its two N and two U nearest neighbour ions; other ions are only slightly perturbed. (b) and (c) are plotted with respect to the N atom and ion respectively (increments are 0.01 and $0.0112e$ Å^{-3}).

and the hole is distributed over first and to a lesser extent second neighbour atoms. Lastly, we find that, once complete lattice relaxation has been performed, the Frenkel and Schottky pair formation energies are very similar. Consequently, intrinsic vacancy and interstitial defects will exist in comparable concentrations so that both are available for mediating defect transport. Recent first principles calculations of ZrN and TiN [23] also predict a local crystal perturbation by vacancies, as do calculations of V_N in AlN [25], despite the fact that AlN has a different crystal structure.

Analysis of the electron density redistribution shows that the effective charge of N atoms depends critically on their position and environment, which limits the applicability of MD simulations based on formal invariant charged species [11] to studies of defects in nitrides.

Acknowledgments

Computing resources for NJA and RWG were provided by the MOTT2 facility (EPSRC Grant GR/S84415/01). We are indebted to P van Uffelen, H Matzke, A M Stoneham, C Ronchi, R Konings, V V Rondinella, Th Gouder and R Caciuffo for many stimulating discussions.

References

[1] Matzke Hj 1986 *Science of Advanced LMFBR Fuels* (Amsterdam: North-Holland)
[2] Matzke Hj 1992 *Diffusion Processes in Nuclear Materials* (Amsterdam: Elsevier)
[3] Blank H 1992 *Nuclear Materials* vol 10A *Nonoxide Ceramic Nuclear Fuels* ed B R T Frost (New York: VCH)
[4] *Proc. Global 2005 Conf. on Future Reactor Technologies (Tsukuba, Japan, Oct. 2005)*
[5] Catlow C R A 1977 *Proc. R. Soc.* A **353** 533
[6] Jackson R A, Murray A D, Harding J H and Catlow C R A 1986 *Phil. Mag.* A **53** 27
[7] Grimes R W and Catlow C R A 1991 *Phil. Trans. R. Soc.* A **335** 609
[8] Crocombette J-P, Jollet F, Nga T and Petit T 2001 *Phys. Rev.* B **64** 104107
[9] Freyss M, Petit T and Crocombette J-P 2005 *J. Nucl. Mater.* **347** 44 and references therein
[10] Brooks M S S and Glötzel D 1980 *Physica* B **102** 51
Brooks M S S and Glötzel D 1984 *J. Phys. F: Met. Phys.* **14** 639
[11] Kurosaki K, Yamada K, Uno M, Yamanaka S, Yamamoto K and Namekawa T 2001 *J. Nucl. Mater.* **294** 160–7
[12] Kresse G and Hafner J 2003 Computer code *VASP Guide* University of Vienna

[13] Segall M D, Lindan P J D, Probert M J, Pickard C J, Hasnip P J, Clark S J and Payne M C 2002 *J. Phys.: Condens. Matter* **14** 2717
[14] Perdew J P and Wang Y 1992 *Phys. Rev.* B **45** 13244
[15] Monkhorst H J and Pack J D 1976 *Phys. Rev.* B **13** 5188
[16] Staun Olsen J, Gerward L and Benedict U 1985 *J. Appl. Crystallogr.* **18** 37
[17] Henkelman G, Arnaldsson A and Jonsson H 2006 *Comput. Mater. Sci.* **36** 254
[18] Rafaja D, Havela L, Kuzel R, Wastin F, Colineau E and Gouder T 2005 *J. Alloys Compounds* **386** 87
[19] Bradbury M H and Matzke Hj 1978 *J. Nucl. Mater.* **75** 68
[20] Kudin K, Scuseria G E and Martin R L 2002 *Phys. Rev. Lett.* **89** 266401
[21] Masaki N and Tagawa H 1975 *J. Nucl. Mater.* **58** 241
[22] Rundle R E, Baenziger N C, Wilson A S and McDonald R A 1948 *J. Am. Ceram. Soc.* **70** 99
Le Bihan T, Idiri M and Heathman S 2003 *J. Alloys Compounds* **358** 120
[23] Ashley N J, Grimes R W and McClellan K J 2006 *J. Mater. Sci.* at press
[24] Greenwood N N 1968 *Ionic Crystals Lattice Defects and Nonstoichiometry* (London: Butterworths) p 72
[25] Vail J M *et al* 2004 *J. Phys.: Condens. Matter* **16** 3371
Vail J M, Chevrier D K, Pandey R and Blanco M A 2006 *J. Phys.: Condens. Matter* **18** 2125